HHS Public Access

Author manuscript

J Neurosci Res. Author manuscript; available in PMC 2023 December 04.

Published in final edited form as:

J Neurosci Res. 2022 November ; 100(11): 2044–2054. doi:10.1002/jnr.25118.

Quantification of functional recovery in a larval zebrafish model of spinal cord injury

Darius Hossainian[1,2], **Enhua Shao**[1,2,3], **Binxuan Jiao**[1,2,3], **Vladimir A. Ilin**[1,2], **Ritika S. Parris**[1,2], **Yangzhong Zhou**[1,2,3], **Qing Bai**[1,2], **Edward A. Burton**[1,2,4,*]

[1]Department of Neurology, University of Pittsburgh School of Medicine, Pittsburgh, PA, 15213, USA

[2]Pittsburgh Institute for Neurodegenerative Diseases, University of Pittsburgh School of Medicine, Pittsburgh, PA, 15213, USA

[3]Tsinghua University Medical School, Beijing, China

[4]Geriatric Research, Education and Clinical Center, Pittsburgh VA Healthcare System, Pittsburgh, PA, 15213, USA

Abstract

Human spinal cord injury (SCI) is characterized by permanent loss of damaged axons, resulting in chronic disability. In contrast, zebrafish can regenerate axonal projections following CNS injury and re-establish synaptic contacts with distant targets; elucidation of the underlying molecular events is an important goal with translational potential for improving outcomes in SCI patients. We generated transgenic zebrafish with GFP-labeled axons and transected their spinal cords at 10 days post-fertilization. Intravital confocal microscopy revealed robust axonal regeneration following the procedure, with abundant axons bridging the transection site by 48 hours post-injury. In order to analyze neurological function in this model, we developed and validated new open-source software to measure zebrafish lateral trunk curvature during propulsive and turning movements at high temporal resolution. Immediately following spinal cord transection, axial movements were dramatically decreased caudal to the lesion site, but preserved rostral to the injury, suggesting the induction of motor paralysis below the transection level. Over the subsequent 96 hours, the magnitude of movements caudal to the lesion recovered to baseline, but the rate of change of truncal curvature did not fully recover, suggesting incomplete restoration of caudal strength over this time course. Quantification of both morphological and functional recovery following SCI will be important for the analysis of axonal regeneration and

*Corresponding author: 7015 Biomedical Sciences Tower 3, 3501 Fifth Avenue, Pittsburgh, PA 15213 - 3301, USA, eab25@pitt.edu.

Author contributions:

Conceptualization (DH, ES, BJ, VAI, RSP, YZ, QB, EAB); methodology (DH, ES, BJ, VAI, RSP, YZ, QB, EAB); software (DH, VAI, YZ); validation (DH); formal analysis (DH, ES, EAB); investigation (DH, ES, BJ, VAI, QB); resources (QB, EAB); writing - original draft (DH); writing - review & editing, supervision, project administration, funding acquisition (EAB).

Conflict of interest statement:

The authors have no conflicts of interest.

Supporting information

1. The attached document contains supplemental figures and tables, and instructions for installing and operating the software.
2. The attached .zip archive contains the MATLAB files necessary to run the tracking analyses reported in this manuscript.
3. The attached .XLSX file contains the source data for figures 3 – 5.

downstream events necessary for restoration of motor function. An extensive array of genetic and pharmacological interventions can be deployed in the larval zebrafish model to investigate the underlying molecular mechanisms.

Keywords

axonal regeneration; swimming kinematics; spinal paralysis; intravital microscopy; high-speed macrovideography; machine vision

Introduction

Spinal cord injury (SCI) is an intractable clinical problem with severe impacts on functional capacity and long-term quality of life. Current treatments are directed at preventing medical complications (such as urosepsis, decubitus ulcers and venous thromboembolism), but have little impact on neurological outcomes (reviewed in (Cadotte and Fehlings 2011)). Cord transection or crush injury in both SCI patients and mammalian SCI models causes ascending and descending spinal cord axons to undergo Wallerian degeneration. These axons do not regrow, resulting in permanent motor, sensory and autonomic deficits below the level of the lesion (Thomas et al. 1997). There is an urgent and unmet need for treatments that promote restoration of axonal projections and neurological recovery in SCI patients.

Unlike the situation in mammals, subsets of adult zebrafish spinal cord axons regenerate following cord injury (Becker et al. 1997) leading to partial recovery of motor function (van Raamsdonk et al. 1998). The mechanisms underlying this inter-species difference may be informative for identifying molecular targets with translational potential in SCI patients, and consequently are under intense investigation. Both cell-intrinsic properties of neurons and a permissive tissue environment are thought to support axonal regeneration in the zebrafish CNS (reviewed in (Rasmussen and Sagasti 2017)). Previous work in adult zebrafish SCI and optic nerve regeneration models demonstrated that neuronal expression of genes such as L1.1 cell adhesion molecule (Becker et al. 2004) and α1-tubulin (regulated by KLF6/7 (Veldman et al. 2010)) contribute to cell-intrinsic mechanisms favoring axonal regrowth. CNS tissue environment factors encouraging axonal regrowth include axonal growth-promoting properties of the zebrafish homologue of Nogo-A, a prominent myelin-derived inhibitory signal in mammals (Welte et al. 2015); absent post-injury upregulation of chondroitin sulfate, a component of the inhibitory glial scar in mammals (Becker and Becker 2002); promotion of spinal axonal growth by neuropeptide-Y expressed on motor neurons (Cui et al. 2021); and glial bridge formation mediated by *fgf* (Goldshmit et al. 2012) and *ctgfa* (Mokalled et al. 2016), allowing axons to cross the injury site.

Adult zebrafish SCI models are time-consuming, technically challenging, and low throughput. Furthermore, the full range of powerful genetic and chemical biology tools available for analyzing zebrafish models is more readily applicable in larvae. Consequently, recent studies have focused on larval zebrafish spinal cord transection models (Bhatt et al. 2004; Briona et al. 2015; Ohnmacht et al. 2016), in which neuronal and axonal regeneration occur rapidly and can be observed directly by intravital microscopy. Importantly, genetic

(Keatinge et al. 2021) and chemical biology (Chapela et al. 2019) approaches can be applied in these models to resolve underlying molecular mechanisms and identify putative therapeutics. Recent studies using larval SCI models have yielded insights into molecular mechanisms, implicating *dbx1a*-expressing radial glia in neurogenesis following injury (Briona and Dorsky 2014); innate immunity and dopaminergic signaling in promoting regeneration of segmental spinal motor neurons (Ohnmacht et al. 2016); neuronal cAMP in stimulating reticulospinal axonal growth (Bhatt et al. 2004); peripheral macrophage-derived anti-inflammatory signals in the permissive tissue environment for axonal bridging at the level of the lesion (Tsarouchas et al. 2018); Wnt/β-catenin signaling both in neurogenesis (Briona et al. 2015) and in the deposition of collagen XII that allows axons to grow across the injury site (Wehner et al. 2017); and Tgf-β in preventing the inhibition of axonal growth by inflammatory Il-1 signaling (Keatinge et al. 2021). The latter study in particular used rapid, high throughput reverse genetics to define molecular mechanisms unequivocally – a unique strength of zebrafish models.

The translational value of putative therapeutic interventions identified in these models will be dependent on their capacity to restore function. Consequently, it is critical to include neurological endpoints in studies of regeneration following SCI. Previous work in larval zebrafish SCI models employed assays such as swimming distance (Ohnmacht et al. 2016) or proportion of animals showing a motor response (Briona and Dorsky 2014) following mechanosensory stimuli to the tail, kinematics of the startle response following water jet stimulus to the tail (Bhatt et al. 2004), or high resolution analysis of truncal swim waves in head-restrained zebrafish (Vasudevan et al. 2021). These approaches depend on eliciting responses in each zebrafish individually, and consequently are time-consuming and potentially susceptible to inter-trial stimulus variability and observer bias. A caudal mechanical stimulus also does not distinguish loss of responses resulting from sensory versus motor deficits. A high-throughput machine vision method measuring swimming distance and change in orientation during the dark phase of a repeated light-dark cycle provided quantitative outputs suitable for chemical screening (Chapela et al. 2019). However, these endpoints are an indirect marker of spinal paralysis that might be incompletely sensitive to the clinical deficits that typify SCI. Activity measurements of this type are also susceptible to modulation by extraneous factors such as direct muscle injury and systemic consequences of injury.

In view of these limitations, the aim of the present study was to quantify the initial motor deficits and subsequent recovery following transection of descending motor axons in a larval zebrafish model. We developed a new open-source MATLAB application to analyze swimming kinematics at high spatiotemporal resolution in experimental groups and controls simultaneously. We found that truncal curvature dynamics mediating turning and propulsive movements were severely disrupted below the level of an acute spinal transection at 10 days post-fertilization. These abnormalities recovered progressively during the 4 days following injury. However, even 48 hours after abundant regenerated axons were seen bridging the lesion site, motor recovery was incomplete. The approach and resources we report will facilitate evaluation of the mechanisms mediating functional recovery, improve screening approaches by providing unbiased quantitative assay outputs sensitive to spinal cord

function, and enhance translational studies by focusing on clinically relevant neurological endpoints.

Materials and Methods

Ethical approval:

All studies were carried out with approval from the University of Pittsburgh Institutional Animal Care and Use Committee, in accordance with the NIH *Guide for the Care and Use of Laboratory Animals*.

Experimental subjects:

The study involved larval zebrafish at 10 days post-fertilization, which were bred in-house. Zebrafish sex is not established at this developmental point and so the study included subjects with potential to differentiate into either sex. To label spinal cord axons for intravital imaging, we employed Tg(*UAS:GFP-CAAX*)^{ue102} zebrafish (Munzel et al. 2012); when crossed to a Gal4 driver, this line expresses GFP fused to the CAAX signal from the human HRas protein, resulting in CAAX-directed farnesylation and membrane anchoring of GFP. To activate transgene expression specifically in neurons, Tg(*UAS:GFP-CAAX*) zebrafish were crossed with Tg(*eno2:gal4FF*)^{pt425} driver zebrafish (Xie et al. 2020), which express a truncated form of Gal4-VP16 with minimal toxicity (Distel et al. 2009), under transcriptional control of neuronal *cis*-regulatory elements from the *eno2* gene that express strongly in the projection neurons of interest (Bai et al. 2007; Bai et al. 2009). The double transgenic zebrafish were further crossed onto the *Casper* background (White et al. 2008) to abolish pigment formation and facilitate intravital microscopy. Embryos were raised in E3 buffer (5mM NaCl, 0.17mM KCl, 0.33mM $CaCl_2$, 0.33mM $MgSO_4$) in an incubator at 28.5° C, with white light illumination (200 lx, 14 hours light:10 hours dark) to 5 days post-fertilization (dpf) then transferred to 1-liter tanks with continual water flow and three times daily feeding with brine shrimp and dried feed.

Experimental design and procedures:

Spinal cord transection: At 10 dpf, zebrafish were individually anesthetized in 0.015% buffered tricaine in E3 for 1 – 2 minutes then transferred to a 35mm surgery dish with a layer of silicone (Sylgard, Corning) at the bottom covered by E3 buffer. Zebrafish were positioned by direct visualization under a dissecting microscope to expose a lateral view of the trunk, and gently prevented from drifting using forceps. The spinal cord was located by fluorescence signal and anatomical landmarks and transected level with the caudal extremity of the swim bladder. A stylet was made from 0.016-inch (≈ 0.41mm) diameter tungsten wire that was sharpened to a fine point by electrolysis (Brady 1965) then attached to a wooden handle. The stylet was inserted through the skin and spinal cord of the zebrafish in a single pass and immediately withdrawn to minimize trauma to muscle and surrounding tissues. The zebrafish was then transferred to a plate with fresh E3 solution to recover for 1 hour prior to further testing.

Intravital imaging: Zebrafish larvae were anesthetized in 0.015% tricaine, placed on one side in a 35mm glass bottom dish (MatTek, Ashland, MA), and immobilized in 50μL of

2% low melting point agarose in E3 to prevent movement, as reported previously (Van Laar et al. 2020). Z-planes encompassing the entire depth of the spinal cord and adjacent tissues were acquired from below through the glass coverslip, using an Olympus IX-81 inverted microscope with a 20x objective (UPlanSApo, NA 0.75) and Fluoview confocal system (B&B Microscopes, Pittsburgh, PA). Maximum projection images of the Z-stack are shown in the figures. Immediately image capture was completed, agarose was removed from around the zebrafish using forceps, and the zebrafish recovered E3 buffer, allowing sequential imaging of spinal axons over several days.

Visual motor responses: To facilitate downstream image processing, zebrafish were housed in wells cut into an agarose-filled plate. The similar IR transmission of agarose and embryo water ensured that the edges of each behavioral arena were not visible in the video stream. Briefly, 0.3% agarose was poured into a single-well plate to a depth of 6 – 7mm (approximately half the interior height of the plate) and allowed to solidify. Wells of 15mm diameter, arranged as 6 rows of 4 wells, were made using a circular cutter and filled with E3 buffer, so that menisci were not present. A single zebrafish was transferred to each well and allowed to acclimatize for 30 minutes. Assays were carried out inside an incubator at 28.5°C to maintain constant temperature and prevent unintentional exposure to extraneous stimuli. Visual motor responses were elicited by transitions between 2-minute periods of bright white light (1100 lx, 4900K) and 1 second periods of dark (<1 lx; “dark flash”). Illumination was provided by LEDs (Super Bright LEDs, St. Louis, MO; cat #LSM-CW3X3), controlled by a USB relay (EtherTek Circuits, Princeton, BC, Canada). Recordings for analysis of motor responses were made over 40 stimulus cycles. Between recordings, zebrafish were housed socially within experimental groups in 1L tanks.

Video capture: Video was captured from below the plate using infrared illumination (#BL812-880, Spectrum Illumination, Montague, MI), and a high-speed camera (Integrated Design Tools, Pasadena, CA; model #NX8-S2) with a macro lens (Rokinon 100mm f2.8; B&H, New York) and infrared-pass filter (R72, 720nm; B&H) to allow videography independent of ambient visible illumination. Uncompressed video segments were captured for 1 second at 1000 frames/s, triggered by the same USB relay used to control the white LEDs, in order to synchronize recording with stimulus. Recordings were analyzed offline using custom MATLAB scripts (see below and supplemental data).

Data and statistical analysis:

Statistical analyses were carried out using GraphPad Prism version 9.4.0. Data were normally distributed by D’Agostino and Pearson test, allowing use of parametric statistical tests. Linear regression was used to compare manually and computationally derived angles. One sample t-tests were employed to compare the differences between manually and computationally derived angles to 0. For quantitative kinematic analysis, zebrafish without detectable responses at each time point (overall 1/120 control wells and 37/120 SCI wells over 5 days of recordings) were removed from analysis instead of being assigned values of 0, in order to avoid artificially inflating the effect of SCI on truncal curvature during VMR responses. 20/1440 individual data points were removed as they exceeded acceptable thresholds for tracking errors or were statistical outliers (ROUT, Q=1%). Two-way ANOVA

with Šidák *post hoc* test was used to compare control and SCI zebrafish at multiple time points.

Results

Regeneration of spinal axons in a larval zebrafish model of spinal cord injury

Using intravital microscopy, we investigated axonal regeneration in a larval zebrafish spinal cord transection model at 10 days post-fertilization (dpf; figure 1). Tg(*eno2:gal4FF*)^{pt425}; Tg(*UAS:GFP-CAAX*)^{ue102}; *mpv17*$^{-/-}$; *mitfa*$^{-/-}$ zebrafish larvae (Munzel et al. 2012; White et al. 2008; Xie et al. 2020) were generated (figure 1A, B) to express membrane-bound GFP within large projection neurons (Bai et al. 2007; Bai et al. 2009), on a background lacking pigment, thereby allowing direct visualization of labeled spinal cord axons *in vivo* by confocal microscopy (figure 1B, D). We transected the spinal cord at a level adjacent the caudal swim bladder using a tungsten stylet under tricaine anesthesia at 10 dpf. Zebrafish were imaged both before the injury, and at intervals afterwards (figure 1C), allowing verification of the cord transection and direct observation of regeneration (figure 1D). Immediately after injury, a large void in the spinal cord GFP signal was evident at the lesion site, reflecting transection of axons passing through the damaged spinal segments, and mechanical disruption of neurons located at this level (figure 1D). By 24 hours post-injury (hpi), isolated axons were seen entering the transection site. Between 24 and 48 hpi, substantial axonal regrowth occurred, so that by 48 hpi large bundles of longitudinally oriented axons were seen bridging the injury site (figure 1D). Together, these data suggest that regeneration of ascending and/or descending spinal cord axons is both robust and rapid in this model.

Measuring swimming kinematics at high spatiotemporal resolution

We next asked if spinal cord transection resulted in a detectable motor deficit below the level of the lesion, and whether the observed axonal regeneration led to functional recovery. To accomplish this, we employed the zebrafish visual-motor response (VMR), in which an abrupt change in ambient illumination from light to dark causes a stereotypical high-angle turning movement termed an ‘O’-bend (Burgess and Granato 2007a). Importantly, this response is dependent on retinal and diencephalic photoreceptors whose responses activate spinal motor neurons indirectly via descending spinal axons (Fernandes et al. 2012). Consequently, the afferent limb of the reflex is not impacted by spinal cord injury, so the assay output reflects the function of the recovering descending spinal motor axons.

To record the VMR, video was captured from below the zebrafish at 1000 frames/s for 1s during a dark flash (figure 2A). Figure 2B shows an example response in which a zebrafish larva at 10 dpf made two high angle turning movements in response to the stimulus. We developed an application to quantify truncal curvature during the VMR, using a similar conceptual approach to work reported previously (Burgess and Granato 2007a), but differing in two ways. First, the application was written using MATLAB for compatibility with our previously reported open-source zebrafish neurological phenotyping tools (Scheetz et al. 2018; Zhou et al. 2014). Second, the method was optimized for simultaneous analysis of multiple larvae, each housed in separate chambers, to facilitate comparison between

different experimental groups exposed in parallel to the same stimuli. The software files/source code and operating manual are provided in supplemental data.

Output from the tracking application is illustrated in figure 2C and D (which show the initial turning movement made by the zebrafish in figure 2B) and its logic is detailed in supplemental figure 1. In each video frame, the program locates a zebrafish in each well of a multi-well plate, identifies the head, and draws a bar from the center of the head caudally, along a vector overlying the darkest pixels of the image corresponding to the zebrafish (head bar; red in figure 2D). A second bar (body; green) of identical length is similarly drawn from where the first bar ends, and a third bar (tail; blue) is drawn from the distal end of the second bar. The result is a 3-segment line that overlies the long axis of the zebrafish. The line is straight when the zebrafish is at rest, but when muscle contraction causes lateral truncal curvature during swimming movements, the line segments form three angles, ∡head-tail, ∡head-body and ∡body-tail. These angles increase with truncal curvature and can be used to quantify the magnitude and rate of lateral trunk bending. For each well in each frame of the video, the result of a frame-by-frame image subtraction to identify motion events is written to an output file, together with the (*x, y*) coordinates of the larval head, the orientation of each bar, and the ∡head-tail, ∡head-body and ∡body-tail angles. Additional calculations yield larval displacement and speed, and the angular velocity of truncal curvature. The measured and calculated parameters together provide a detailed picture of activity, displacement, and truncal curvature dynamics for each zebrafish following each stimulus (figure 2E shows the complete response for the zebrafish in figure 2B).

Observation of several hours of the live tracking output from the algorithm by multiple different observers showed that the three body segment lines were reliably located over the long axis of the zebrafish. We validated the algorithm quantitatively against manual determination of truncal curvature. An additional application was developed allowing an observer to draw lines of constrained length (representing head, body, and tail bars to mimic the algorithm) manually onto video frames that did not show the automatically generated bars. This approach was highly replicable in images of a resting zebrafish, with 100 consecutive trials showing variability of 0.019 ± 0.006 rad. We next added body segment bars manually to every 5th video frame spanning entire movement episodes in 20 different zebrafish (figure 3A). There was a strong correlation ($R^2 = 0.991$, $p < 0.0001$) between trunk angles calculated from the automatically generated and manually determined bar positions; quantitative analysis showed an overall error of 0.013 ± 0.006 rad and the mean absolute error was 0.084 rad (= 4.8°; figure 3B). We employed the same method to add bars manually to video frames corresponding to the maximum trunk curvature for a further 74 movement episodes (figure 3C). Similarly, this showed a very strong correlation between manual and automatic angular assignments ($R^2 = 0.995$, $p < 0.0001$), such that the overall error of 0.009 ± 0.016 rad did not differ significantly from 0, and the absolute error for measurement of these peak angles was 0.088 rad (= 5.0°; figure 3C). Together, these data show that the new MATLAB application produced robust outputs that describe truncal curvature accurately during larval movement, allowing us to analyze the functional recovery of zebrafish following spinal cord injury.

Swimming kinematics following SCI

We next asked whether larval kinematics during 'O'-bend responses were altered following spinal cord transection (figure 4). Zebrafish underwent spinal cord transection at 10 dpf then motor function assays were carried out daily for 5 days, in comparison with control uninjured sibling zebrafish (figure 4A). Responses to 40 dark flashes of 1s duration, each preceded by 2-minutes of bright white light ambient illumination, were recorded each day.

Response rates to stimuli differed between the injured and uninjured zebrafish (figure 4B). Between 10 – 14 dpf, control zebrafish produced movements within 1s of the light-dark transition, consistently after 55 – 65% stimuli. Response rate was dramatically decreased immediately after spinal cord transection (control 54.3 ± 4.6 % vs. injury 3.0 ± 1.5%, $p<0.0001$, 2-way ANOVA with Šidák *post hoc* test, n = 24/group). There was some recovery over the next 48 hours (immediate post injury 3.0 ± 1.5% *vs.* 2 days post-injury 28.6 ± 5.6%, p=0.0077), but the response rate remained lower in the injury group for the duration of the experiment. Consequently, the groups differed significantly even at 4 days post-injury (control 59.2 ± 5.4% *vs.* injury 24.5 ± 6%, p<0.0001). These data show that spinal cord transection provoked a dramatic and long-lasting decrease in the probability of a motor response to dark flash stimulus.

Even though the probability of response was reduced, it was still possible to capture movement episodes in many of the injured zebrafish (9/24 immediately post-injury; 19/24 at 4 days post-injury). Figure 3C shows video frames corresponding to baseline and maximum trunk angle for control and injured zebrafish, immediately post-injury, and 4 days post-injury. The baseline images in both groups and timepoints show a straight trunk without spinal deformity. In response to stimuli, control zebrafish at both time points show similar high-angle curvature involving the entire trunk. In contrast, immediately after spinal cord transection, there was truncal curvature proximal to the injury, but no movement distal to the lesion, likely reflecting paralysis of muscles below the transected spinal level (arrow). At 4 days post-injury, truncal curvature following dark flash stimulus was similar to the control. These images suggest that – similar to mammalian models – zebrafish with acute spinal cord lesions have a 'motor level' with a severe neurological deficit caudal to the injury. Importantly this appeared to recover over several days.

We next quantified these observations using the new MATLAB application (figure 5, supplemental figure 2, supplemental tables 1 – 6). Trunk curvature (figure 5A; ∡head-tail) was decreased immediately post injury (control 2.0 ± 0.07 *vs.* injury 0.94 ± 0.13 rad, $p<0.0001$, 2-way ANOVA with Šidák *post hoc* test). As predicted from inspection of the video images, ∡head-body was preserved (figure 5B; control 0.87 ± 0.04 *vs.* injury 0.82 ± 0.12 rad, $p=0.9981$), but there was a dramatic decrease in ∡body-tail (figure 5C; control 1.14 ± 0.03 *vs.* injury 0.38 ± 0.04 rad, $p<0.0001$). The maximal body-tail angle gradually recovered and did not differ significantly from control by 4 days post-injury (control 1.11 ± 0.05 vs. injury 1.05 ± 0.05 rad, p=0.9628). Interestingly, ∡head-body also gradually increased in the injury group, so that it was significantly higher than control at 4 days post-injury (control 0.87 ± 0.07 vs. injury 1.27 ± 0.06, p=0.0003). This may represent a compensatory response to the impaired truncal movements caused by the injury.

Finally, we used changes in the frame-by-frame angular measurements to calculate angular velocity of trunk curvature, as a marker of muscle contraction force. This is important, as the maximum trunk angle potentially could be preserved even in the presence of weaker, slower, muscle contractions. The maximal trunk angular velocity was dramatically decreased immediately post-injury (control 66.4 ± 2.3 vs. injury 38.5 ± 3.2 rad/s, p<0.0001) but recovered rapidly and had reached baseline by 4 days post-injury (control 66.8 ± 1.8 vs. injury 65.8 ± 2.1 rad/s, p=0.9998). There was a modest decrease in head-body angular velocity immediately post-injury (control 48.5 ± 1.3 vs. injury 38.6 ± 3.5 rad/s, p=0.0114) but this recovered rapidly and was similar to control by 4 days post-injury (control 55.5 ± 1.1 vs. injury 53.0 ± 2.1 rad/s, p=0.8616). In contrast, body-tail angular velocity was dramatically decreased immediately post injury (control 69.3 ± 2.0 vs. injury 40.2 ± 3.8 rad/s, p<0.0001). Although substantial recovery was noted during the time course of the experiment, body-tail angular velocity in SCI zebrafish remained modestly reduced and significantly lower than control even 4 days after the injury (control 79.2 ± 1.5 vs. injury 69.1 ± 1.6, p=0.0094). Notably, modest changes in both maximum angle and angular velocity occurred in the control group at 11 – 14dpf relative to 10dpf (supplemental figure 3). This suggests that age-matched cohort controls (as employed here) are the appropriate comparison group for these experiments.

Together, these data show acute loss of motor function below the level of spinal cord transection in this model. Functional recovery starts rapidly and continues after the appearance of regenerated axons bridging the lesion site at 2 dpi, but measurable motor deficits are still detected at 4 dpi.

Discussion:

Previous studies reported larval zebrafish SCI at 5 dpf; we selected a later developmental point for several reasons. Most importantly, the spinal cord is closer to an adult configuration at 10 dpf than at 5 dpf; for example, myelination is well underway, and markers of mature myelin such as P0 are expressed in long tracts (Bai et al. 2011). Studying this later time point may help distinguish mechanisms mediating regeneration from ongoing development. Indeed, this is a common criticism of larval models (Rasmussen and Sagasti 2017), although many molecular mechanisms may be shared between development and regeneration (Cardozo et al. 2017). In combination with our tungsten stylet method, the larger size of the zebrafish at 10 dpf also allowed spinal lesions to be induced with minimal damage to surrounding tissues and without using antibiotics (that might alter assay outcomes) to prevent infections during recovery. In addition, the body length difference between 5 dpf and 10 dpf necessitates axonal regrowth over a longer distance, providing a more stringent test of regeneration. By using a mutant lacking pigment and labeling spinal axons with membrane bound GFP, we were able to extend the time window for intravital imaging of axonal regeneration to this later developmental point. Consequently, although it is necessary to house and feed zebrafish for additional days compared with injury at 5 dpf, the 10 dpf timepoint presents potential advantages and may be useful for both discovery-driven and hypothesis testing approaches.

We report new open-source software to quantify zebrafish trunk curvature in a video recording. The algorithm was validated extensively and provides accurate measurements of truncal dynamics during movement. The three-segment truncal line strategy was based on FLOTE (Burgess and Granato 2007a; Burgess and Granato 2007b), but we implemented this approach in a new MATLAB algorithm for compatibility with our previously reported open-source neurobehavioral phenotyping software (Scheetz et al. 2018; Zhou et al. 2014), and for convenience in downstream analysis as the rich dataset is written directly to MATLAB matrices. We further optimized the application for analyzing multiple zebrafish moving simultaneously in separate wells, to facilitate comparison of treatment and control groups in the same assays. A variety of approaches has been employed previously to analyze zebrafish kinematics, ranging from manual analysis of video recordings (Budick and O'Malley 2000), to sophisticated and fully automated systems, some of which allow real-time analysis of video streams with closed-loop control of stimulus presentation (Guilbeault et al. 2021; Marques et al. 2018; Portugues and Engert 2011; Štih et al. 2019). Several of these solutions analyze truncal curvature across multiple body segments rather than the simpler 3-bar strategy we used here. Although this may provide a more detailed picture of truncal curvature along the rostro-caudal extent of the body axis, these analyses usually require images at a higher magnification than employed here. Consequently, multi-segment applications have mostly found utility in the analysis of complex behaviors in single zebrafish, sometimes in a head-restrained preparation and coupled with calcium imaging. Our approach differs in prioritizing analysis of statistically robust experimental groups and controls responding to simultaneous stimuli, at high temporal resolution, while minimizing the processing power and time necessary for analysis. We predict the new software may be useful for quantifying responses with characteristic kinematic properties in comparative quantitative applications, for example analyzing zebrafish models of neurological diseases relative to controls, or screening for chemical or genetic modifiers of motor phenotypes.

Coupled with high-speed videography of the responses to abrupt light-dark transition, the new application enabled us to quantify the neurological deficits resulting from SCI in larval zebrafish and to document how these recovered over time. The data are of interest for several reasons. First, it is critically important to measure clinically relevant endpoints in disease models, as restoration of morphology or other surrogate markers without meaningful neurological recovery would be of limited value. The hallmark neurological deficit in SCI patients is loss of neurological function below the level of the injury. Our data demonstrate a motor level in larval zebrafish, and our approach allows automated unbiased quantification of this hallmark clinical deficit of SCI in an experimentally tractable model. Second, the delay between axonal bridging at the lesion site and restoration of motor function suggests that additional events downstream of initial axon regrowth are essential for functional recovery. We anticipate these include axonal extension and to spinal segments innervating caudal muscles, and reestablishment of functional synaptic contacts with other neurons at their site of termination. The molecular basis of these processes has received less attention than axonal bridging at the lesion site but is likely critical for clinical recovery. Consequently, a detailed understanding of the molecular mechanisms mediating later events in regeneration after initial axonal growth may be a prerequisite for exploiting zebrafish models for development of therapies. The data also suggest that axonal bridging alone might

not be optimal for evaluating experimental therapeutics, since although axonal regrowth is likely necessary for neurological recovery, it is probably not sufficient. Third, our approach allowed us to detect aspects of motor function that did not recover quantitatively over the time course of these experiments. Although maximum ∡body-tail recovered to baseline, its corresponding angular velocity did not, suggesting ongoing weakness of muscle contraction. It is possible that recovery occurs over a more prolonged time course than evaluated here; however, it is noteworthy that even after long-term recovery in adult zebrafish SCI models, swimming function is not fully restored to pre-injury levels (van Raamsdonk et al. 1998). Although it is undoubtedly true that any degree of recovery might be worthwhile to patients with permanent and complete paralysis following injury, these observations suggest more rigorous tests of function that could be exploited to discover interventions that enhance recovery from SCI. Finally, our observation that movements rostral to the transection site are increased following paralysis caudal to the injury implies that compensatory mechanisms may tend to restore movement, separate from neurological recovery in the paralyzed segments. Hyperkinesia rostral to the injury took 48 hours to appear and may involve plasticity in the relevant spinal circuitry. It is currently unclear whether this alone could contribute significantly to the apparent improvement in indirect functional endpoints such as quantification of locomotor vectors following SCI.

Our findings are overall complementary to an elegant analysis reported recently, in which motor recovery was quantified in individual head-restrained zebrafish larvae after SCI at 5dpf (Vasudevan et al. 2021). Forward swimming movements were provoked by visual moving bar stimuli at 3- and 9-days post-injury, and trunk curvature was analyzed in 20 segments from swim bladder to tail, allowing quantification of propagating swim waves both rostral and caudal to the lesion site. Compatible with our data, these experiments showed decreased power and peak frequency in the power spectra of swim waves caudal to the injury, which resolved over the time course of the experiment. Interestingly, a persistent increase in power was also observed rostral to the injury, supporting the idea that hyperkinesia in uninjured segments may represent a compensatory response.

High-throughput motor assays have recently been used to test chemical modifiers of recovery from SCI, with clear translational implications (Chapela et al. 2019). Our new data extend this approach by providing means to quantify how chemical modifiers mitigate the hallmark neurological deficit of SCI in a larval zebrafish model. Consequently, we predict that the resources we report here will be useful, both for studies on molecular mechanisms of functional recovery from SCI in zebrafish, and in translational studies to test putative therapeutic interventions.

Supplementary Material

Refer to Web version on PubMed Central for supplementary material.

Acknowledgements:

This work was supported by NINDS (NS058369), the Ethel Vincent Charitable Trust, and UPMC. ES, BJ and YZ were Tsinghua University Scholars at the University of Pittsburgh and were supported by the Chinese Research Council. RSP was supported by an NIH training grant (AG21885). VAI current address: UPMC Graduate Medical

Education, Pittsburgh, PA, 15213. RSP current address: Department of Internal Medicine, Beth Israel Deaconess Hospital, Boston, MA. We thank the aquatics team at the University of Pittsburgh Department of Laboratory Animal Resources for expert care of our transgenic zebrafish lines.

Data accessibility:

The data and new software that support the findings of this study are available in the supplementary material of this article.

References

Bai Q, Garver JA, Hukriede NA, Burton EA. 2007. Generation of a transgenic zebrafish model of Tauopathy using a novel promoter element derived from the zebrafish eno2 gene. Nucleic acids research 35(19):6501–6516. [PubMed: 17897967]

Bai Q, Sun M, Stolz DB, Burton EA. 2011. Major isoform of zebrafish P0 is a 23.5 kDa myelin glycoprotein expressed in selected white matter tracts of the central nervous system. J Comp Neurol 519(8):1580–1596. [PubMed: 21452240]

Bai Q, Wei X, Burton EA. 2009. Expression of a 12-kb promoter element derived from the zebrafish enolase-2 gene in the zebrafish visual system. Neurosci Lett 449(3):252–257. [PubMed: 19007858]

Becker CG, Becker T. 2002. Repellent guidance of regenerating optic axons by chondroitin sulfate glycosaminoglycans in zebrafish. J Neurosci 22(3):842–853. [PubMed: 11826114]

Becker CG, Lieberoth BC, Morellini F, Feldner J, Becker T, Schachner M. 2004. L1.1 is involved in spinal cord regeneration in adult zebrafish. J Neurosci 24(36):7837–7842. [PubMed: 15356195]

Becker T, Wullimann MF, Becker CG, Bernhardt RR, Schachner M. 1997. Axonal regrowth after spinal cord transection in adult zebrafish. J Comp Neurol 377(4):577–595. [PubMed: 9007194]

Bhatt DH, Otto SJ, Depoister B, Fetcho JR. 2004. Cyclic AMP-induced repair of zebrafish spinal circuits. Science 305(5681):254–258. [PubMed: 15247482]

Brady J 1965. A simple technique for making very fine, durable dissecting needles by sharpening tungsten wire electrolytically. Bull World Health Organ 32(1):143–144. [PubMed: 20604205]

Briona LK, Dorsky RI. 2014. Radial glial progenitors repair the zebrafish spinal cord following transection. Exp Neurol 256:81–92. [PubMed: 24721238]

Briona LK, Poulain FE, Mosimann C, Dorsky RI. 2015. Wnt/ss-catenin signaling is required for radial glial neurogenesis following spinal cord injury. Dev Biol 403(1):15–21. [PubMed: 25888075]

Budick SA, O'Malley DM. 2000. Locomotor repertoire of the larval zebrafish: swimming, turning and prey capture. J Exp Biol 203(Pt 17):2565–2579. [PubMed: 10934000]

Burgess HA, Granato M. 2007a. Modulation of locomotor activity in larval zebrafish during light adaptation. J Exp Biol 210(Pt 14):2526–2539. [PubMed: 17601957]

Burgess HA, Granato M. 2007b. Sensorimotor gating in larval zebrafish. J Neurosci 27(18):4984–4994. [PubMed: 17475807]

Cadotte DW, Fehlings MG. 2011. Spinal cord injury: a systematic review of current treatment options. Clin Orthop Relat Res 469(3):732–741. [PubMed: 21080129]

Cardozo MJ, Mysiak KS, Becker T, Becker CG. 2017. Reduce, reuse, recycle - Developmental signals in spinal cord regeneration. Dev Biol 432(1):53–62. [PubMed: 28502615]

Chapela D, Sousa S, Martins I, Cristovao AM, Pinto P, Corte-Real S, Saude L. 2019. A zebrafish drug screening platform boosts the discovery of novel therapeutics for spinal cord injury in mammals. Sci Rep 9(1):10475. [PubMed: 31324865]

Cui C, Wang LF, Huang SB, Zhao P, Chen YQ, Wu YB, Qiao CM, Zhao WJ, Shen YQ. 2021. Adequate expression of neuropeptide Y is essential for the recovery of zebrafish motor function following spinal cord injury. Exp Neurol 345:113831. [PubMed: 34363807]

Distel M, Wullimann MF, Koster RW. 2009. Optimized Gal4 genetics for permanent gene expression mapping in zebrafish. Proc Natl Acad Sci U S A 106(32):13365–13370. [PubMed: 19628697]

Fernandes AM, Fero K, Arrenberg AB, Bergeron SA, Driever W, Burgess HA. 2012. Deep brain photoreceptors control light-seeking behavior in zebrafish larvae. Curr Biol 22(21):2042–2047. [PubMed: 23000151]

Goldshmit Y, Sztal TE, Jusuf PR, Hall TE, Nguyen-Chi M, Currie PD. 2012. Fgf-dependent glial cell bridges facilitate spinal cord regeneration in zebrafish. J Neurosci 32(22):7477–7492. [PubMed: 22649227]

Guilbeault NC, Guerguiev J, Martin M, Tate I, Thiele TR. 2021. BonZeb: open-source, modular software tools for high-resolution zebrafish tracking and analysis. Sci Rep 11(1):8148. [PubMed: 33854104]

Keatinge M, Tsarouchas TM, Munir T, Porter NJ, Larraz J, Gianni D, Tsai HH, Becker CG, Lyons DA, Becker T. 2021. CRISPR gRNA phenotypic screening in zebrafish reveals pro-regenerative genes in spinal cord injury. PLoS Genet 17(4):e1009515. [PubMed: 33914736]

Marques JC, Lackner S, Felix R, Orger MB. 2018. Structure of the Zebrafish Locomotor Repertoire Revealed with Unsupervised Behavioral Clustering. Curr Biol 28(2):181–195 e185. [PubMed: 29307558]

Mokalled MH, Patra C, Dickson AL, Endo T, Stainier DY, Poss KD. 2016. Injury-induced ctgfa directs glial bridging and spinal cord regeneration in zebrafish. Science 354(6312):630–634. [PubMed: 27811277]

Munzel EJ, Schaefer K, Obirei B, Kremmer E, Burton EA, Kuscha V, Becker CG, Brosamle C, Williams A, Becker T. 2012. Claudin k is specifically expressed in cells that form myelin during development of the nervous system and regeneration of the optic nerve in adult zebrafish. Glia 60(2):253–270. [PubMed: 22020875]

Ohnmacht J, Yang Y, Maurer GW, Barreiro-Iglesias A, Tsarouchas TM, Wehner D, Sieger D, Becker CG, Becker T. 2016. Spinal motor neurons are regenerated after mechanical lesion and genetic ablation in larval zebrafish. Development 143(9):1464–1474. [PubMed: 26965370]

Portugues R, Engert F. 2011. Adaptive locomotor behavior in larval zebrafish. Front Syst Neurosci 5:72. [PubMed: 21909325]

Rasmussen JP, Sagasti A. 2017. Learning to swim, again: Axon regeneration in fish. Exp Neurol 287(Pt 3):318–330. [PubMed: 26940084]

Scheetz SD, Shao E, Zhou Y, Cario CL, Bai Q, Burton EA. 2018. An open-source method to analyze optokinetic reflex responses in larval zebrafish. J Neurosci Methods 293:329–337. [PubMed: 29042258]

Štih V, Petrucco L, Kist AM, Portugues R. 2019. Stytra: An open-source, integrated system for stimulation, tracking and closed-loop behavioral experiments. PLoS Comput Biol 15(4):e1006699. [PubMed: 30958870]

Thomas CK, Zaidner EY, Calancie B, Broton JG, Bigland-Ritchie BR. 1997. Muscle weakness, paralysis, and atrophy after human cervical spinal cord injury. Exp Neurol 148(2):414–423. [PubMed: 9417821]

Tsarouchas TM, Wehner D, Cavone L, Munir T, Keatinge M, Lambertus M, Underhill A, Barrett T, Kassapis E, Ogryzko N, Feng Y, van Ham TJ, Becker T, Becker CG. 2018. Dynamic control of proinflammatory cytokines Il-1beta and Tnf-alpha by macrophages in zebrafish spinal cord regeneration. Nat Commun 9(1):4670. [PubMed: 30405119]

Van Laar VS, Chen J, Zharikov AD, Bai Q, Di Maio R, Dukes AA, Hastings TG, Watkins SC, Greenamyre JT, St Croix CM, Burton EA. 2020. alpha-Synuclein amplifies cytoplasmic peroxide flux and oxidative stress provoked by mitochondrial inhibitors in CNS dopaminergic neurons in vivo. Redox Biol 37:101695. [PubMed: 32905883]

van Raamsdonk W, Maslam S, de Jong DH, Smit-Onel MJ, Velzing E. 1998. Long term effects of spinal cord transection in zebrafish: swimming performances, and metabolic properties of the neuromuscular system. Acta Histochem 100(2):117–131. [PubMed: 9587624]

Vasudevan D, Liu YC, Barrios JP, Wheeler MK, Douglass AD, Dorsky RI. 2021. Regenerated interneurons integrate into locomotor circuitry following spinal cord injury. Exp Neurol 342:113737. [PubMed: 33957107]

Veldman MB, Bemben MA, Goldman D. 2010. Tuba1a gene expression is regulated by KLF6/7 and is necessary for CNS development and regeneration in zebrafish. Mol Cell Neurosci 43(4):370–383. [PubMed: 20123021]

Wehner D, Tsarouchas TM, Michael A, Haase C, Weidinger G, Reimer MM, Becker T, Becker CG. 2017. Wnt signaling controls pro-regenerative Collagen XII in functional spinal cord regeneration in zebrafish. Nat Commun 8(1):126. [PubMed: 28743881]

Welte C, Engel S, Stuermer CA. 2015. Upregulation of the zebrafish Nogo-A homologue, Rtn4b, in retinal ganglion cells is functionally involved in axon regeneration. Neural Dev 10:6. [PubMed: 25888884]

White RM, Sessa A, Burke C, Bowman T, LeBlanc J, Ceol C, Bourque C, Dovey M, Goessling W, Burns CE, Zon LI. 2008. Transparent adult zebrafish as a tool for in vivo transplantation analysis. Cell Stem Cell 2(2):183–189. [PubMed: 18371439]

Xie W, Jiao B, Bai Q, Ilin VA, Sun M, Burton CE, Kolodieznyi D, Calderon MJ, Stolz DB, Opresko PL, St Croix CM, Watkins S, Van Houten B, Bruchez MP, Burton EA. 2020. Chemoptogenetic ablation of neuronal mitochondria in vivo with spatiotemporal precision and controllable severity. Elife 9.

Zhou Y, Cattley RT, Cario CL, Bai Q, Burton EA. 2014. Quantification of larval zebrafish motor function in multiwell plates using open-source MATLAB applications. Nature protocols 9(7):1533–1548. [PubMed: 24901738]

Significance statement

Understanding the molecular mechanisms that drive regeneration of the zebrafish spinal cord may lead to treatments for human spinal cord injury (SCI) patients with permanent neurological deficits. Spinal cord transection in larval zebrafish caused caudal motor paralysis that recovered rapidly and quantitatively following the appearance of new axons bridging the lesion site. Our study demonstrates quantification of the hallmark neurological deficit of SCI in a highly experimentally tractable model, allowing analysis of the mechanisms downstream of axonal regeneration that result in functional recovery, and providing relevant functional outcomes for translational studies.

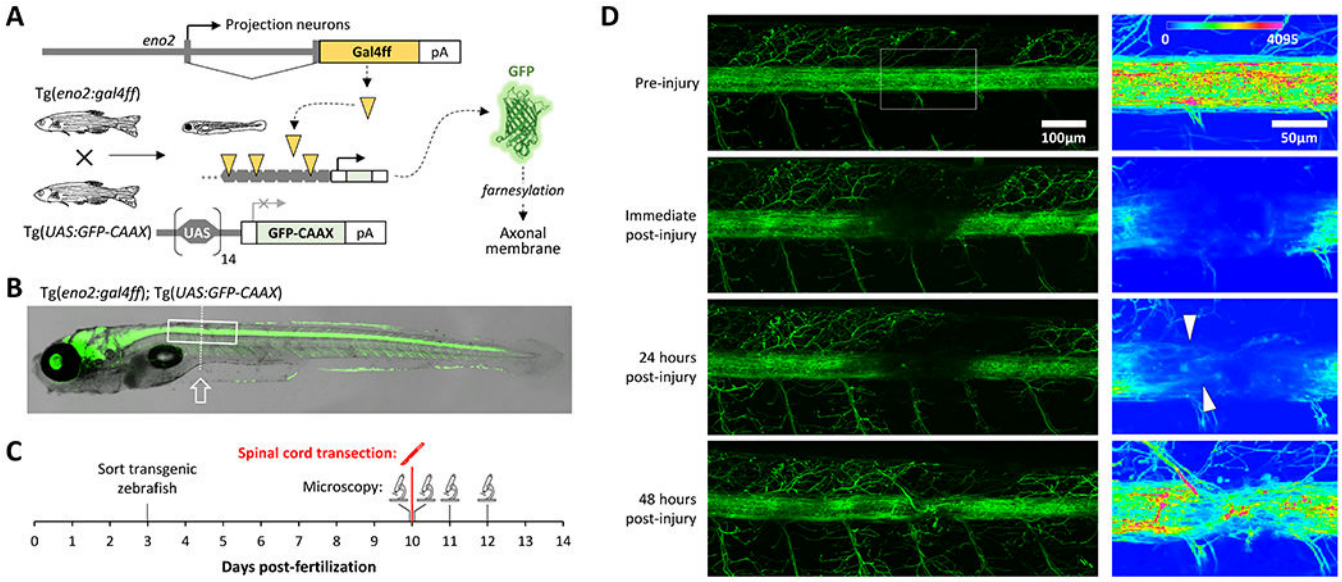

Figure 1: Intravital imaging of axonal regeneration in larval zebrafish

A: Schematic depiction of the transgenic lines used to express GFP at the membrane of ascending and descending spinal axonal projections.

B: Superimposed brightfield and confocal images of a Tg(*eno2:gal4ff*); Tg(*UAS:GFP-CAAX*); *mpv17*$^{-/-}$; *mitfa*$^{-/-}$ zebrafish at 10dpf, illustrating widespread axonal labeling by membrane bound GFP. The boxed area corresponds to the region shown in the left column of panel D and the dotted line indicates the cord transection plane.

C: Time course of the experiment shown in panel D.

D: Confocal Z-plane projections of the spinal cord of a Tg(*eno2:gal4ff*); Tg(*UAS:GFP-CAAX*); *mpv17*$^{-/-}$; *mitfa*$^{-/-}$ zebrafish (rostral is to the left). The same zebrafish was imaged prior to spinal cord transection at 10 dpf (top row of images), immediately afterwards, and 24 and 48 hours later (lower rows). The boxed area in the first image encompassing the transection site is shown at higher magnification in the column of images to the right, using the color intensity scale shown in the top panel. Arrowheads indicate regenerating axons at 24 hours post-injury.

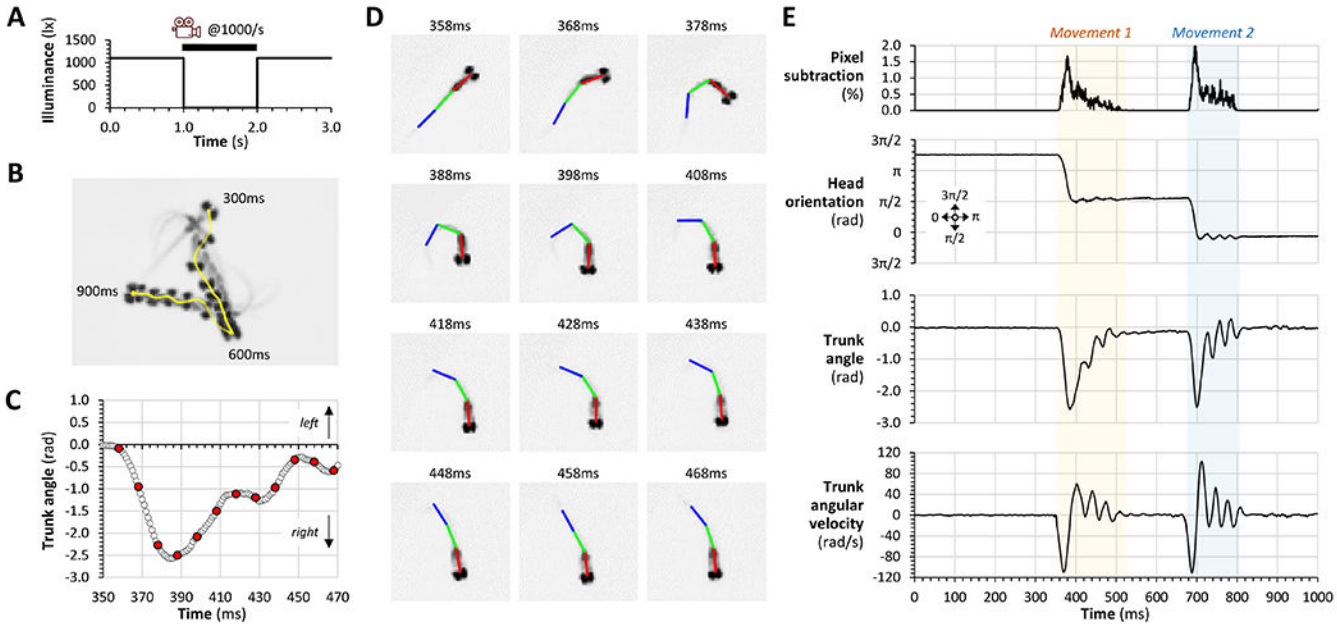

Figure 2: An open-source MATLAB application for quantifying larval zebrafish kinematics following an experimental manipulation

A: Time course of dark flash and camera trigger to elicit and record the VMR.

B: Example response of an individual zebrafish to abrupt light-dark transition. Every 20th video frame from 300ms to 900ms after the stimulus is superimposed to illustrate the changes in larval position and orientation. The vector track of the head centroid during the movement is shown in yellow.

C: The trunk angle (∡head-tail) of the zebrafish in panel B is plotted against time during the first turning movement (350 – 470ms after the stimulus). Red data points correspond to the pictures in panel D.

D: Individual video frames are shown every 10ms between 358 – 468ms after the stimulus. Head (red), body (green) and tail (blue) bars were fitted to the image by the algorithm. Truncal curvature in C and E was by calculated as the angle between the red and blue bars.

E: The entire response over 1000ms is plotted for the zebrafish in panels B – D. Two separate movement episodes are readily identified. In each case the movement started with an abrupt change in larval head orientation, associated with striking truncal curvature, made at high angular velocity in the same direction. The movements conclude with tail-beating motions that cause propulsion.

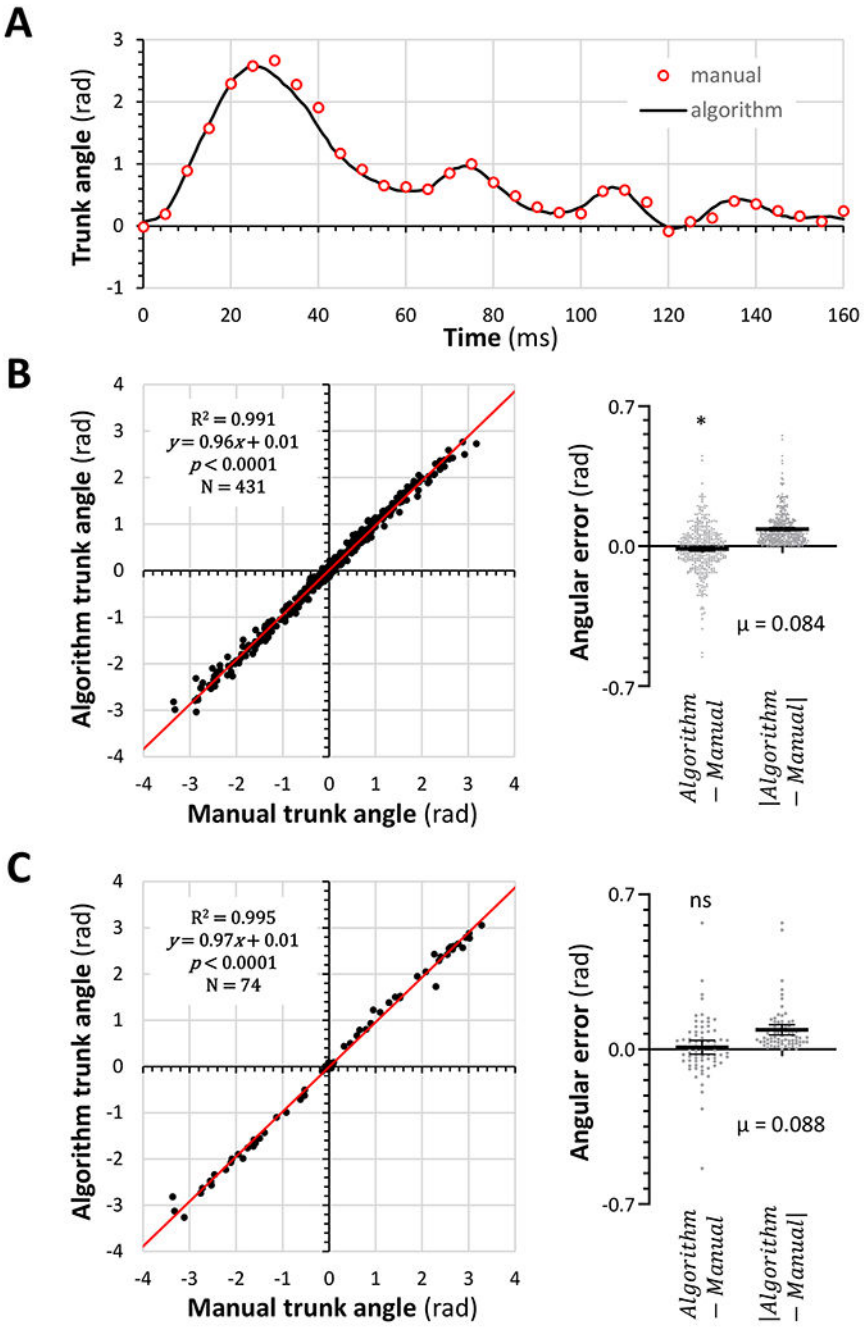

Figure 3: Validation of a MATLAB application for measuring trunk angle dynamically in a high framerate video stream

A: The output from our MATLAB algorithm (solid black line) was compared with trunk angles calculated from manually drawn bars of constrained length mimicking the algorithm in every 5th video frame during a movement episode (red circles) in a zebrafish at 11dpf. B: Trunk angles derived from manually (x-axis) or automatically (y-axis) assigned body segment bars were plotted for 431 video frames corresponding to 20 entire movements similar to the episode shown in panel A. The difference and absolute difference between the manual and automatic measurements is shown in the scatterplots to the right.

C: Similar data to panel B were measured in video frames corresponding to the maximum trunk curvature for 74 separate movement episodes. In B and C, a single sample *t*-test was used to compare the differences between automated and manual measurement to 0 (*$p<0.05$).

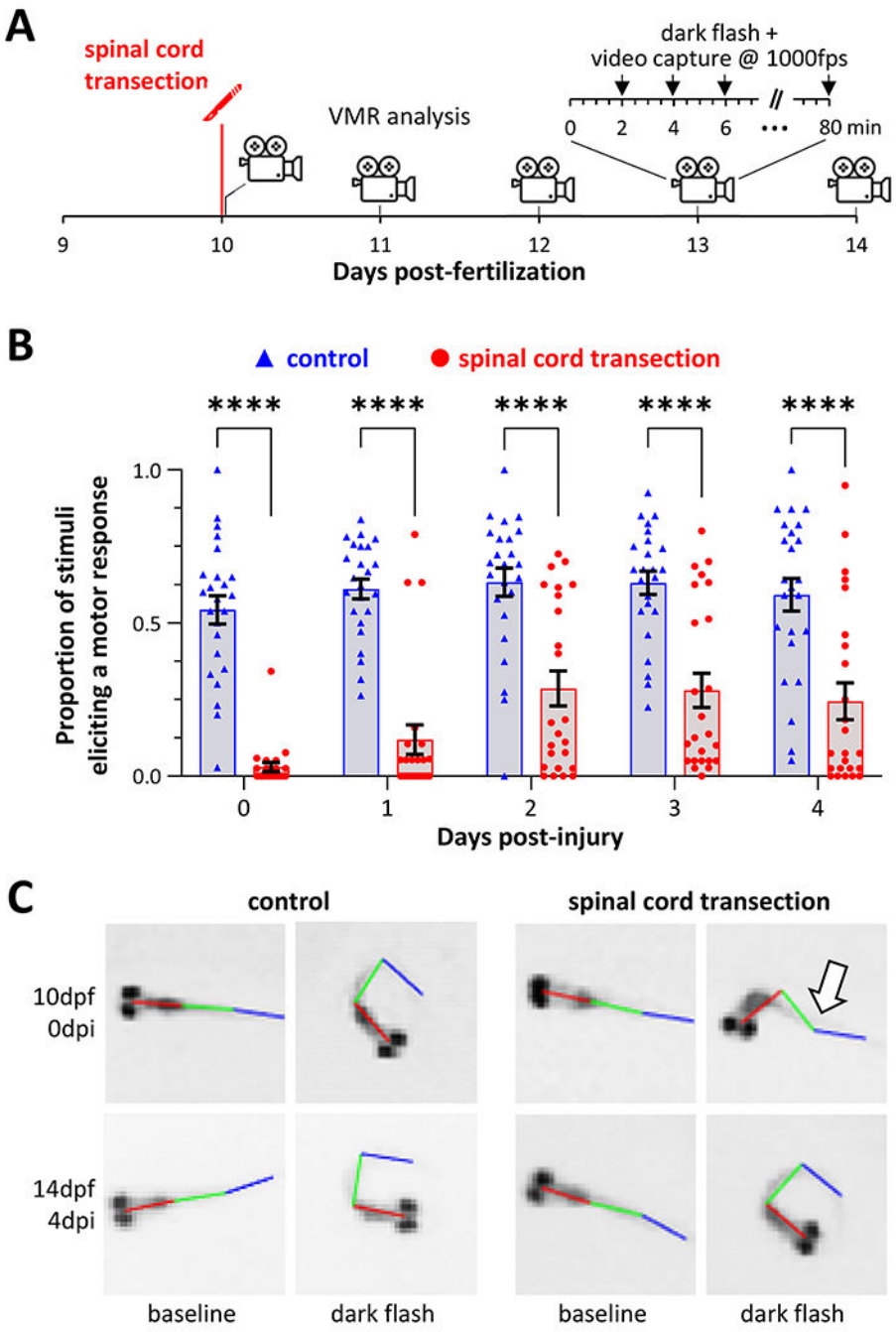

Figure 4: Recovery of reduced response rate and abnormal swimming kinematics following spinal cord transection

A: Time course for the experiments shown in figures 4 and 5. Starting immediately after spinal cord transection, zebrafish motor responses to light-dark transition were recorded daily over 5 days. In each session, responses were recorded to 40 dark flash stimuli each after 2 minutes of acclimatization in bright white light.

B: Response rate (proportion of stimuli that provoked a measurable motor response) is plotted for 24 control (blue) and 24 spinal cord injury (red) zebrafish on each day after injury. ****p<0.0001, 2-way ANOVA with Šidák *post-hoc* test.

C: Representative video frames showing baseline (left column of each group) and maximal (right column of each group) trunk curvature during responses to light-dark transition in control (left group) and spinal cord transection (right group) zebrafish, at 0 (top row) and 4 (bottom row) days post-injury. The arrow indicates the paralyzed distal segment of the injured zebrafish that recovered by 4 days later.

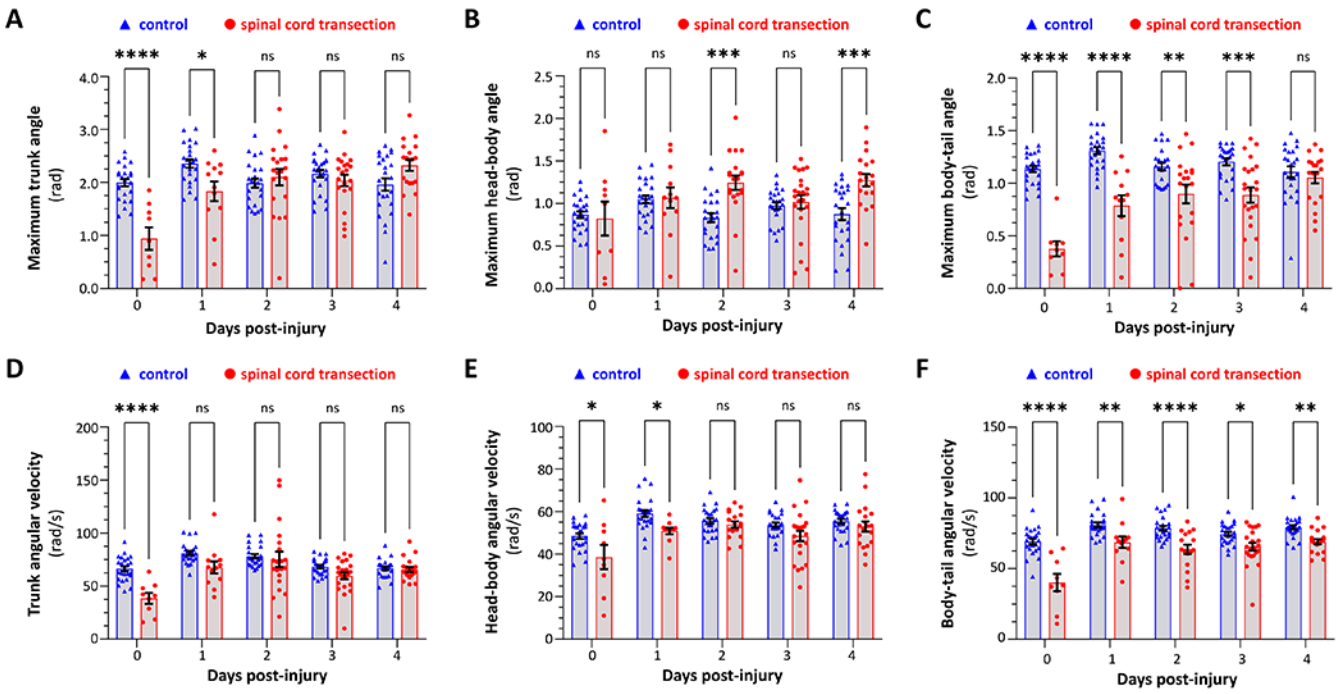

Figure 5: Partial recovery of swimming kinematics following spinal cord transection in larval zebrafish

Kinematics of motor responses to sudden ambient light-dark transition were quantified in control zebrafish (blue, triangles) and siblings that underwent spinal cord transection at 10dpf (red, circles). Data points represent individual zebrafish and show the mean of all elicited responses for each zebrafish at a particular time point (all zebrafish that showed at least one response are included at each time point). Bars show group mean ± SE. A – C show maximal angles: (A) ∡head-tail; (B) ∡head-body; (C) ∡body-tail. D – F show mean angular velocity: (D) head-tail; (E) head-body; (F) body-tail. Data were analyzed by two-way ANOVA with experimental group and time post-injury as variables, and pairwise comparisons made by Šidák post hoc test ($p<0.05$*, 0.001**, 0.0001***, 0.00001****). ANOVA tables are shown in supplemental tables 1 – 6.